Supplementary Information for

Global Patterns of Soil Freeze-Thaw States Below 0 °C

Zhaoyu Dong[1,2], Yuanchao Fan[1,2]*

[1] Institute of Environment and Ecology, Tsinghua Shenzhen International Graduate School, Tsinghua University, Shenzhen, 518055, China.
[2] Key Laboratory of Ecological Carbon Fixation and Sink Enhancement in Ordinary Universities of Guangdong Province, China

*Corresponding Author: Yuanchao Fan
Email: yuanchao.fan@sz.tsinghua.edu.cn

This PDF file includes:

Supplementary Texts 1-2
Supplementary Figures 1 to 13
Supplementary Tables 1 to 5
SI References

Supplementary Text 1: Classification and diurnal asymmetry of SUS events

We classified all SUS events into four categories based on the phase change characteristics observed within ±12 hours relative to the occurrence of each event: consistent thawing (CT), thawing process (TP), freezing process (FP), and diel freeze-thaw alternations (DFT) (see Methods section “Definition of special freeze-thaw events”).

The occurrence times of all SUS events are nearly equally divided to morning and evening hours (06:00 vs. 18:00 local time, 1:1 ratio; Main text Fig. 1d), albeit with notable seasonal variations (Table 1). CT events predominate at both morning/evening time points and across different months. The comparable proportions of TP and FP events (around 5%) across times reflect alternating seasonal influences: from February to May, thawing-driven dynamics prevail as reflected by the increased occurrence of TP events, whereas from October to January, freezing-driven dynamics dominate as reflected by the higher prevalence of FP events. From October to January, the occurrence frequencies of FP and TP events at 6:00 and 18:00 are relatively balanced, with freezing events recorded 2,997,358 times at 6:00 and 3,313,286 times at 18:00, and thawing events recorded 2,946,299 times at 6:00 and 2,911,972 times at 18:00 (Table 1). In contrast, from February to May, a strong diurnal asymmetry emerged, with a substantially higher number of SUS events at 18:00 than 6:00 – FP events increased from 1,805,832 at 6:00 to 3,127,091 at 18:00 (by 73.17%), and TP events increased from 2,064,972 at 6:00 to 3,607,314 at 18:00 (by 74.69%) (Table 1).

The average occurrence soil temperature for each SUS event type follows a general pattern of being lower during the freezing season and higher during the thawing season, with the lowest observed in December (mean values CT: 269.18 K, DFT: 267.93 K, FP: 268.57 K, TP: 268.67 K; Main text Fig. 2g) and highest in May (mean values CT: 272.50 K, DFT: 272.20 K, FP: 272.34 K, TP: 272.45 K; Main text Fig. 2g).

Supplementary Text 2: Differences in daytime and nighttime freeze-thaw temperature patterns

We compared soil temperature and surface (skin) temperature records associated with FP and TP types of SUS events. Given the coarse temporal resolution of freeze–thaw state data and the absence of a threshold for thawing events, we analyzed the average soil temperatures during nighttime (18:00–06:00) and daytime (06:00–18:00) freeze–thaw transitions. This approach allowed us to assess differences between freezing and thawing processes under similar thermal conditions for each time period.

At night, the average soil temperature during the freezing process (269.78 ± 3.70 K) was slightly higher than during the thawing process (269.51 ± 8.92 K; Fig. 7a), a difference that was statistically significant ($t = 112.30$, $p < 0.001$). The median soil temperatures were 270.99 K for freezing and 270.82 K for thawing, respectively, with both distributions displaying negative skewness (–1.95 and –1.81). Binned data analysis further shows that in 84.57% of SM and CEC combinations, the nighttime thawing process occurred at lower soil temperatures than the nighttime freezing process did (Fig. 7b–d).

In contrast, during the daytime, this pattern reversed (Fig. 7e–h). The daytime freezing process occurred at lower average soil temperatures (269.60 ± 3.84 K) than the thawing process did (269.99 ± 10.52 K), with a significant mean difference of 0.39 K ($t = -168.15$, $p < 0.001$). This pattern was observed in 85.23% of SM and CEC combinations. Notably, the standard deviation of soil temperatures during the daytime thawing process (10.52 K) exceeded that of the nighttime thawing process (8.92 K), indicating greater thermal variability and uncertainty during the day.

Supplementary Figures

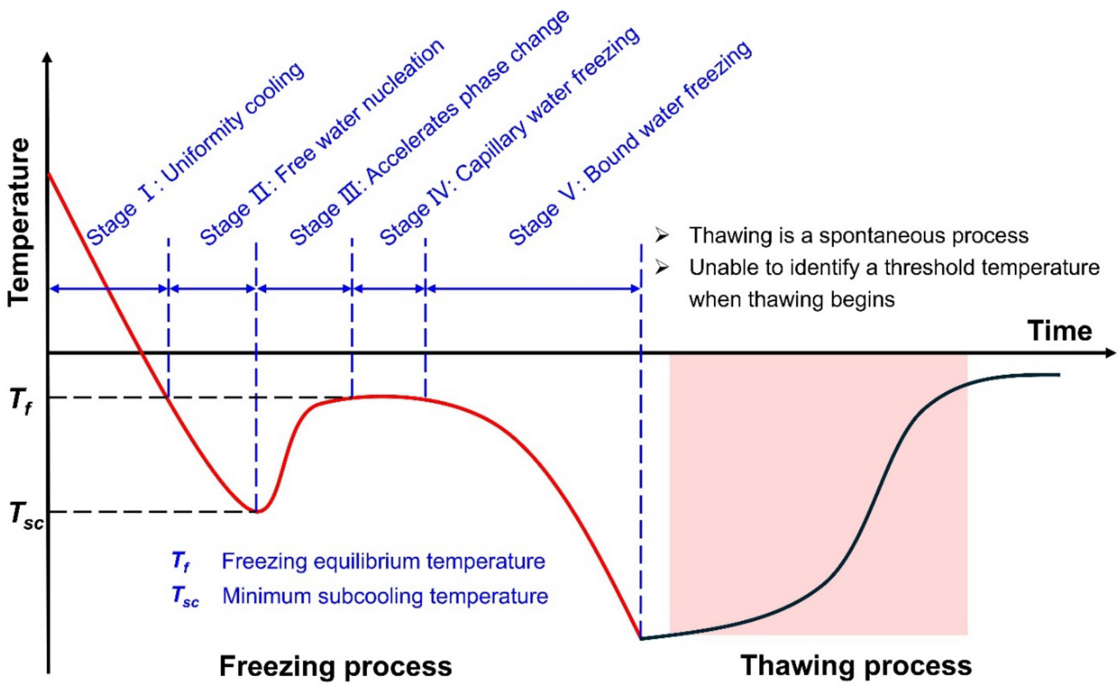

Supplementary Fig. 1 Conceptual diagram of soil freezing and thawing process[1,2,3]. During Stage I, when soil temperature is above the freezing point, no phase change occurs and cooling proceeds uniformly under a stable thermal gradient. Once the temperature drops below the freezing point, Stage II begins, where pore solution nucleates and a small amount of latent heat is released, slowing the cooling rate. With stable nuclei formed, Stage III follows, characterized by rapid ice growth and substantial latent heat release, which temporarily raises the soil temperature and further retards cooling. When the release of latent heat balances external cooling, Stage IV (equilibrium freezing) occurs, during which capillary water and residual free water freeze progressively. Finally, Stage V involves the freezing of bound water at lower temperatures, causing further temperature decline. In contrast, during thawing, external heat directly disrupts the ice crystal structure, and thus no stable, quantifiable melting threshold exists.

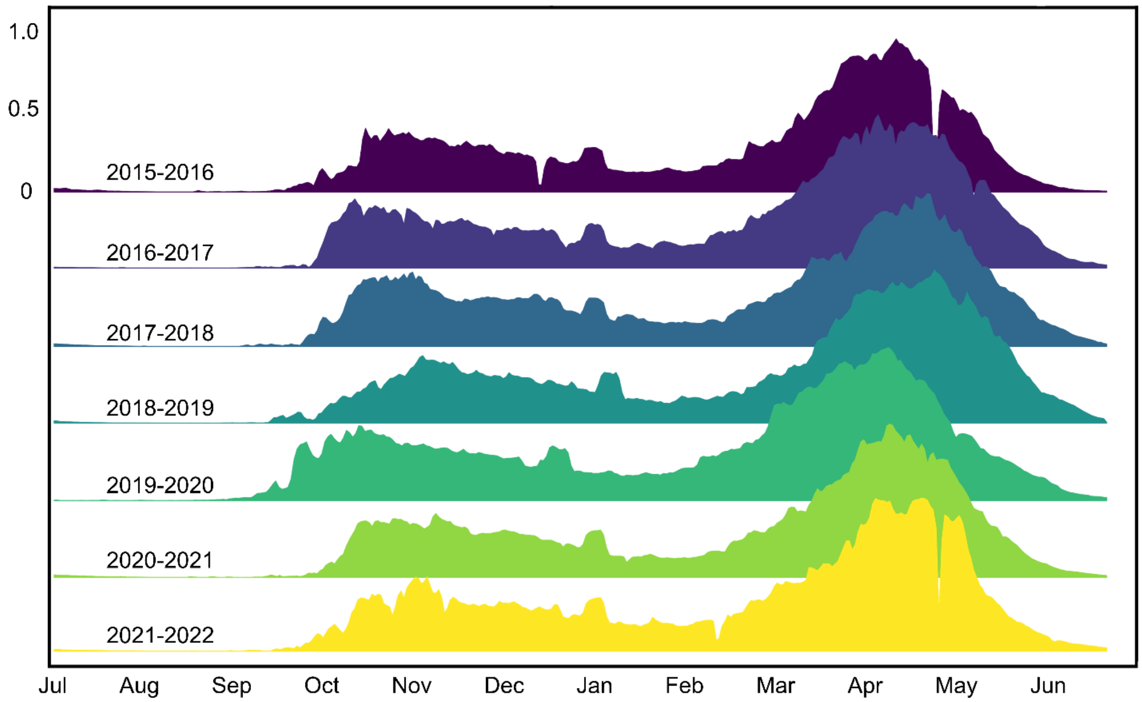

Supplementary Fig. 2 Frequency distribution of SUS events within each annual cycle (July to June) across 2015-2022 (using ERA5 soil temperature[4] and SMAP freeze–thaw state data).

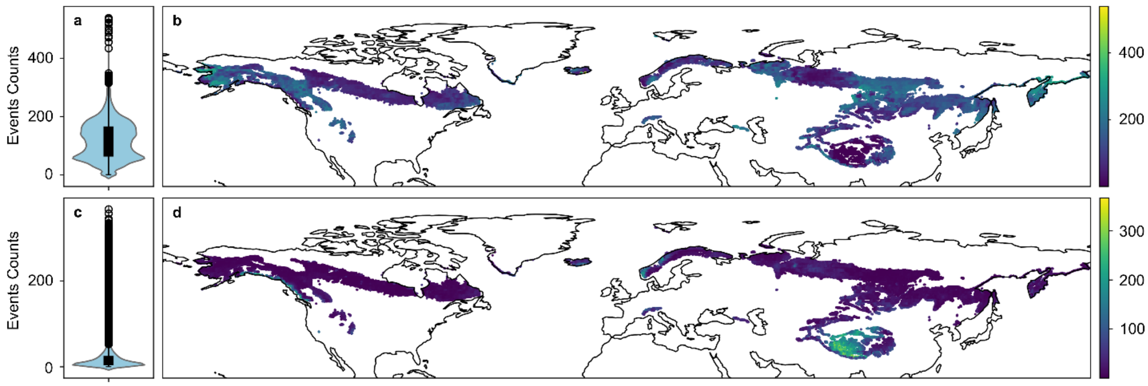

Supplementary Fig. 3 Spatial distribution and statistical characteristics of the annual occurrence of SUS and AFS events. (a) The violin plot shows the average annual counts distribution of SUS events. (b) Spatial distribution of average annual counts of SUS events. (c) Violin plot of the average annual counts of AFS events. (d) Spatial distribution of AFS event occurrences.

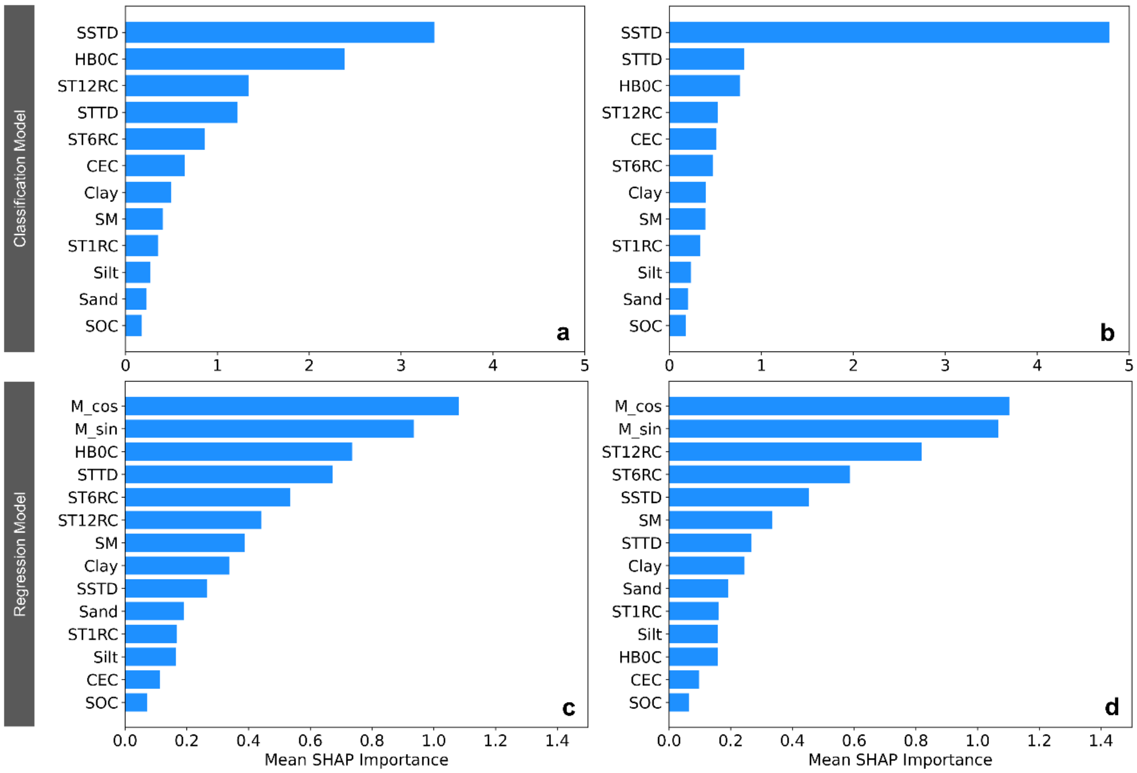

Supplementary Fig. 4 Feature importance rankings for classification and regression models at 6:00 and 18:00. (a) 6:00 Classification Model. (b) 18:00 Classification Model. (c) 6:00 Regression Model. (d) 18:00 Regression Model. Variable abbreviations are defined as follows: SSTD: Soil–Surface Temperature Differential, HB0C: Hours Below 0°C, STTD: Soil Temperature Time Derivative, ST1RC / ST6RC / ST12RC: Soil Temperature Change Rate at 1 / 6 / 12 hours, SM: Soil Moisture, CEC: Cation Exchange Capacity, SOC: Soil Organic Carbon, Clay / Silt / Sand: Soil particle composition, M_sin / M_cos: Sine and Cosine transformations of calendar month.

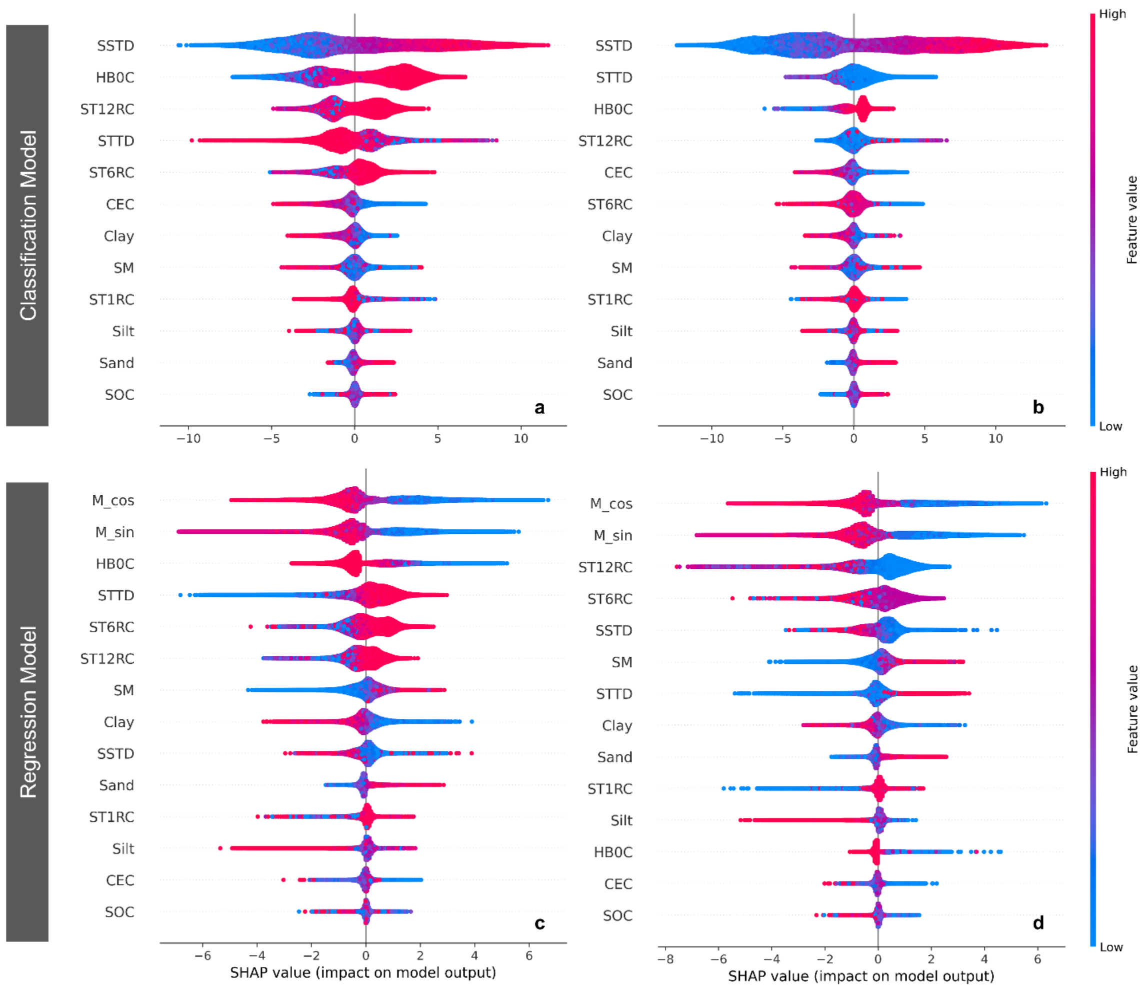

Supplementary Fig. 5 Feature contribution summary plot for classification and regression models at 6:00 and 18:00. (a) 6:00 Classification Model. (b) 18:00 Classification Model. (c) 6:00 Regression Model. (d) 18:00 Regression Model. The horizontal axis denotes the SHAP value from XGBoost model output and the colors (vertical bar) denote input feature values. The feature rankings in a-b are the same as in Fig. 4a, b and those in c-d are the same as in Fig. 4c, d. In the classification model, lower SHAP values indicate feature contributions that increase the likelihood of SUS occurrence. In the regression model, lower SHAP values denote feature effects that reduce SUS event occurrence temperatures.

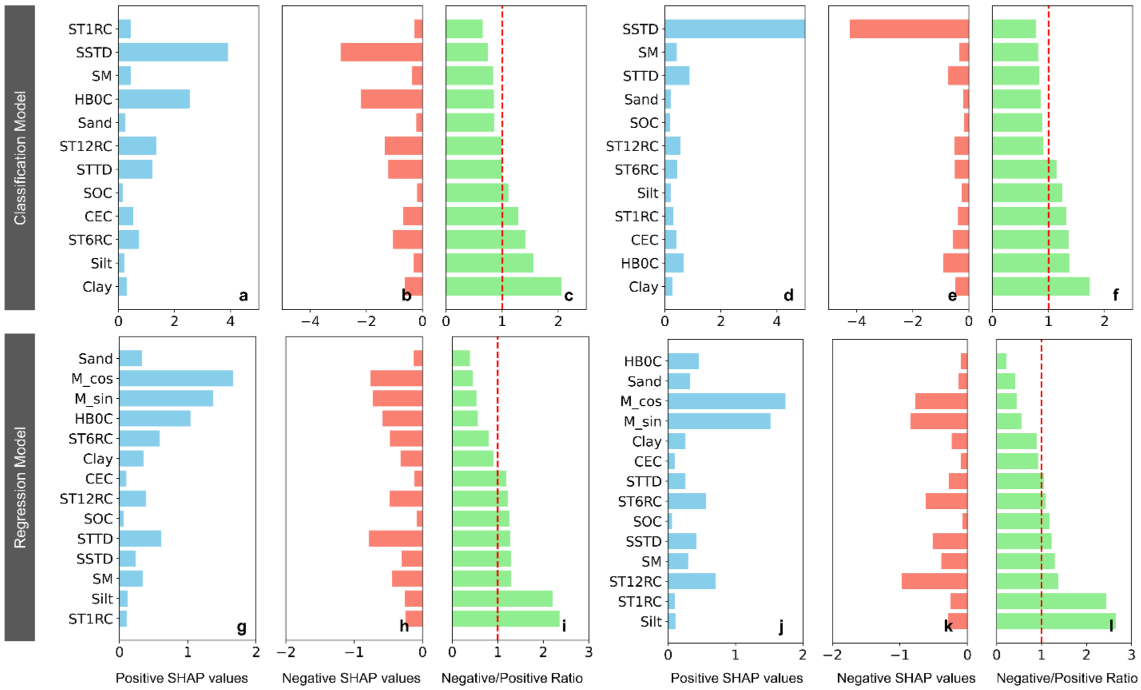

Supplementary Fig. 6 Feature directional contributions and ratios for classification and regression models for SUS events at 6:00 and 18:00, respectively. (a-c) Positive SHAP values, negative SHAP values and the absolute SHAP ratios of (b) divided by (a), respectively, of different features in the XGBoost classification model for 6:00 SUS events. Negative SHAP values in (b) and absolute SHAP ratios > 1 in (c) indicate net contributions of features that promote occurrences of SUS events. (d-f) Positive SHAP values, negative SHAP values and the absolute SHAP ratios of (e) divided by (d), respectively, of different features in the XGBoost classification model for 18:00 SUS events. Negative SHAP values in (e) and absolute SHAP ratios > 1 in (f) indicate freezing-point depression effects of respective features. (g-i) Same as in (a-c) but for the XGBoost regression model for 6:00 SUS events. (j-l) Same as in (d-f) but for the XGBoost regression model for 18:00 SUS events.

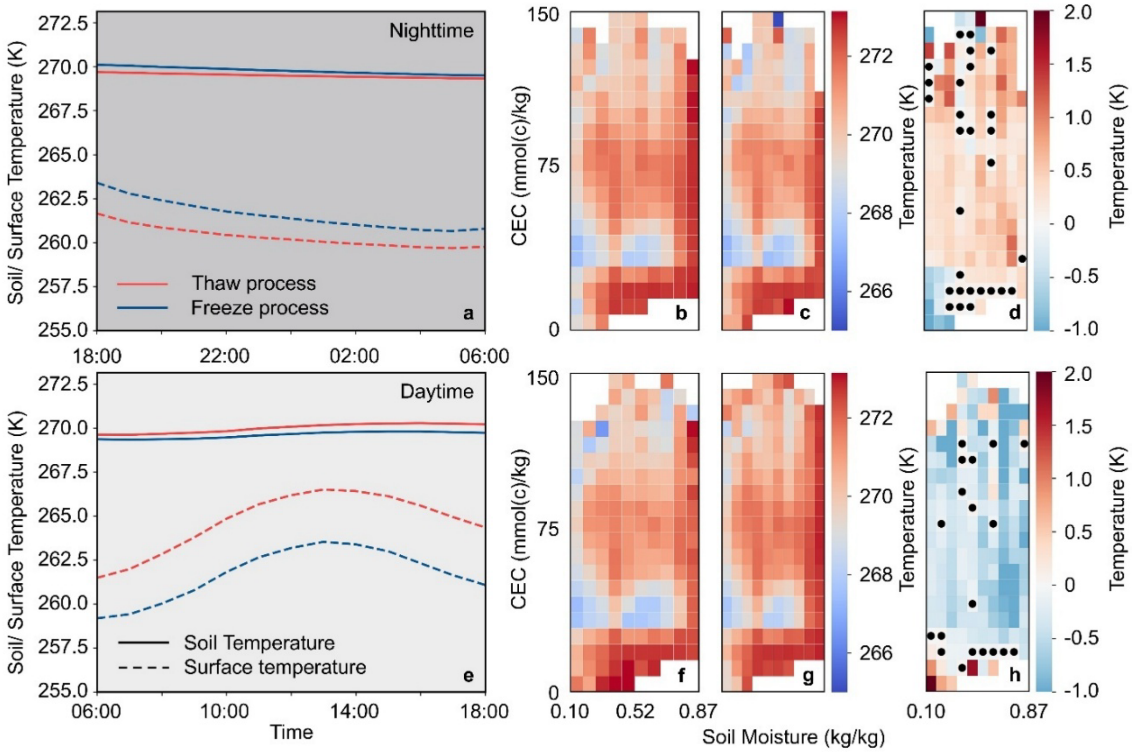

Supplementary Fig. 7 Temperature evolution during freeze–thaw processes of FP and TP SUS events and binned statistics of soil temperatures under different combinations of CEC–SM conditions. (a) Nighttime (18:00 to 06:00) variations in soil temperature (solid lines) and surface temperature (dashed lines) during phase transitions between frozen and thawed states of FP (blue) and TP (red) SUS events. (b) Binned plot of the mean soil temperature for different combinations of soil moisture and CEC gradients during nighttime freezing (FP SUS events). (c) Same as in (b) but during nighttime thawing (TP SUS events). (d) b minus c. (e) Same as in (a) but for daytime (06:00 to 18:00). (f) Same as in (b) but during daytime freezing. (g) Same as in (c) but during daytime thawing. (h) f minus g. The dots in (d) and (h) represent temperature differences less than 0.1K between the corresponding bins.

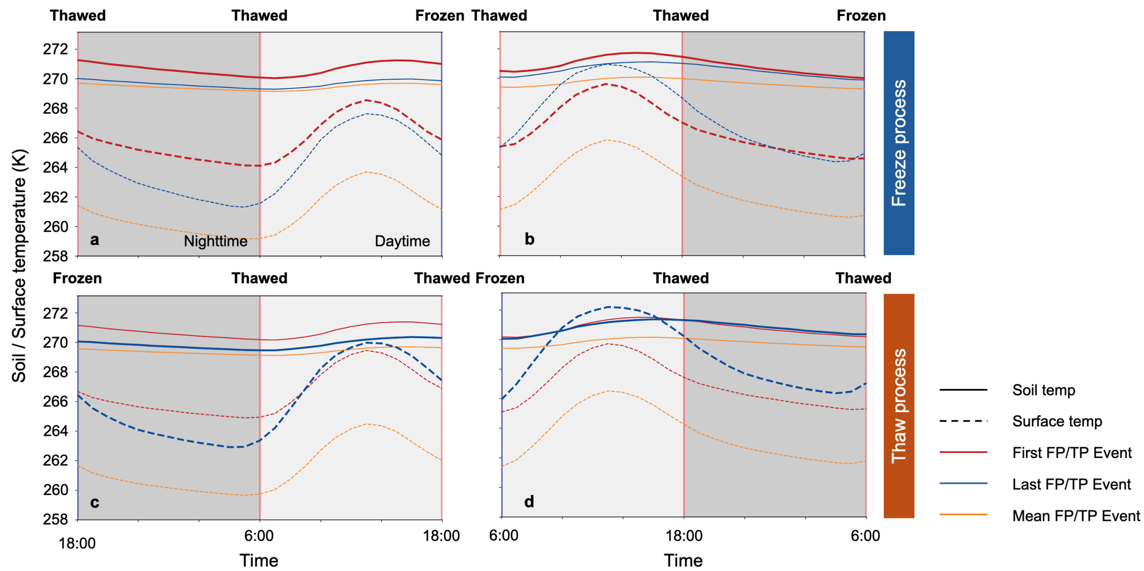

Supplementary Fig. 8 Mean diel dynamics of soil temperature and surface (skin) temperature in all FP and TP type SUS events. (a) Time series of soil and surface temperatures during FP (Thawed→Thawed→Frozen) SUS events at 6:00. (b) Time series of soil and surface temperatures during FP SUS events at 18:00. (c) Time series of soil and surface temperatures during TP (Frozen→Thawed→Thawed) SUS events at 6:00. (d) Time series of soil and surface temperatures during TP SUS events at 18:00. Below Fig. 9 more clearly shows the pattern of supercooling and equilibrium freezing point using a subset of FP type SUS events at 18:00 that have similar occurrence times of latent heat release at freezing.

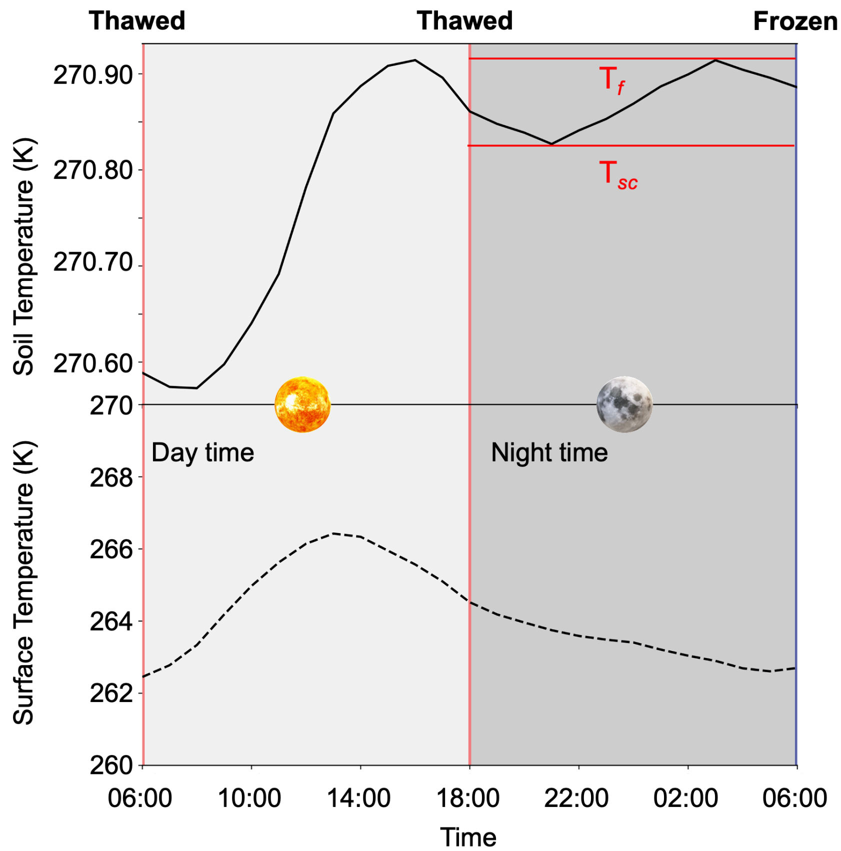

Supplementary Fig. 9 Representative SUS events at 18:00 extracted from Fig. 8b. Notes: Because latent heat release may occur at any time within a 12-hour window and the temporal resolution of the original soil temperature data is 3 hours, the characteristic signals of latent heat release tend to be obscured when calculating mean soil temperature curves over regions with large spatial extents. In this figure, mean soil and surface temperature curves are shown for cases where T_f occurred between 01:00 and 03:00 (local solar time) and T_{sc} occurred before T_f, based on selection of soil temperature sequences where the local minimum precedes the local maximum within a 12-hour window (see Methods).

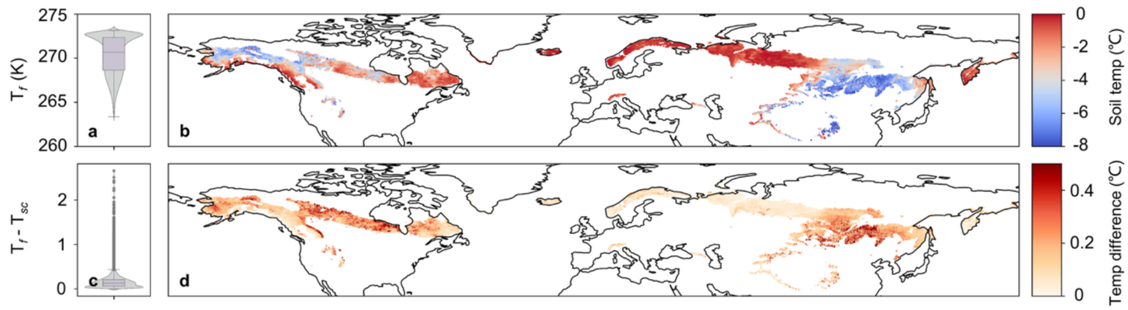

Supplementary Fig. 10 Distribution of SMAP satellite-derived T_f and the difference between T_f and T_{sc} in the Northern Hemisphere. (a) Box plot and violin plot for the distribution of soil freezing temperature (T_f) derived from satellite observations (18:00 FP events). (b) Spatial distribution of multi-year average observed T_f (18:00 FP events). (c) Box plot and violin plot for the distribution of observed T_f minus T_{sc} (18:00 FP events). (d) Spatial distribution of the difference between T_f and T_{sc} (18:00 FP events); T_f - T_{sc} reflects the increase in soil temperature caused by latent heat release.

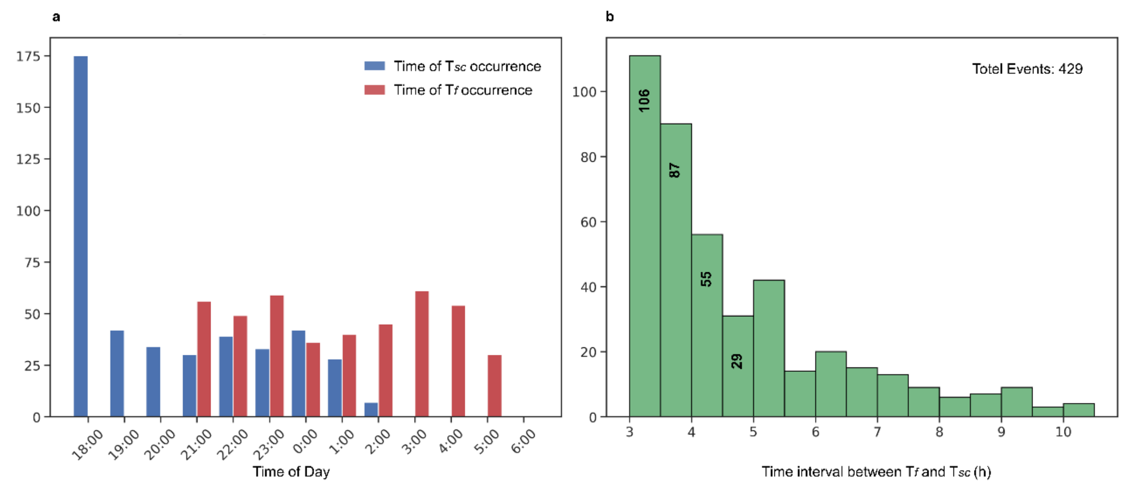

Supplementary Fig. 11 Typical temporal distribution of T_f and T_{sc} and their time intervals during the freezing process at night observed at eddy covariance flux tower sites. The absence of T_{sc} occurring after 2:00 and T_f occurring before 21:00 is to ensure the same minimum time interval as the satellite data as described in the multi-feature freezing point diagnostic framework in Methods.

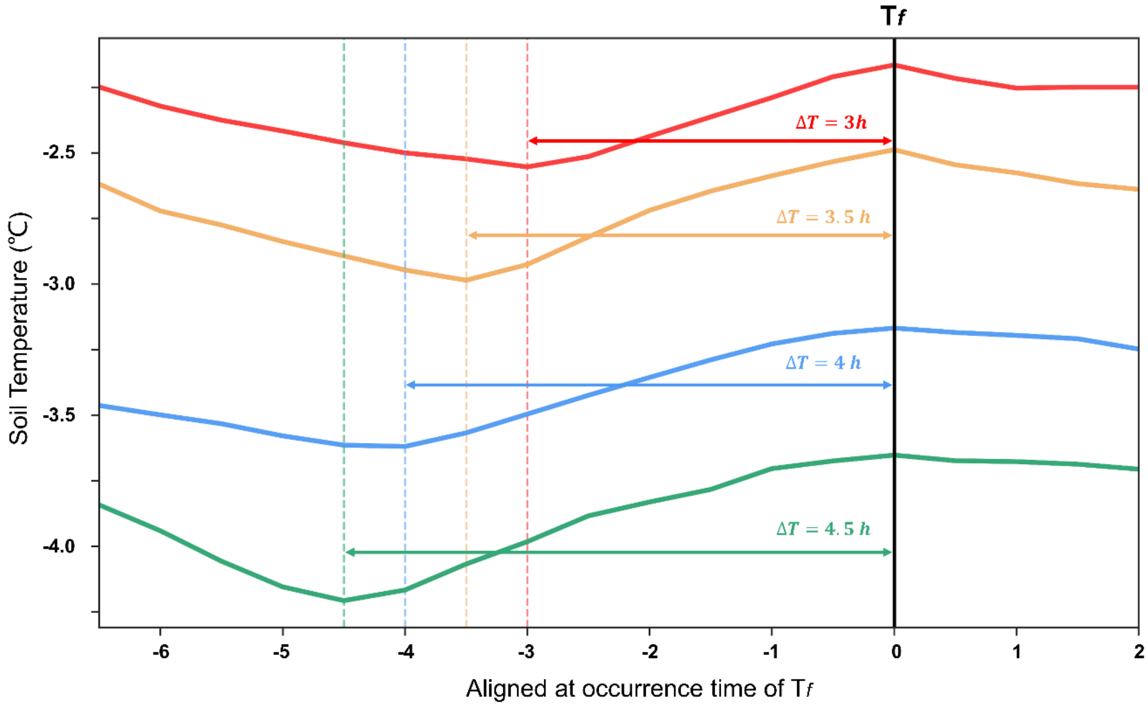

Supplementary Fig. 12 In-situ observations of freezing points across the available flux tower sites. Composite median soil temperature curves aligned at T_f for different T_f–T_{sc} time differences. Events with T_f–T_{sc} time lags between 3 and 4.5 hours account for approximately 64.57% of all samples.

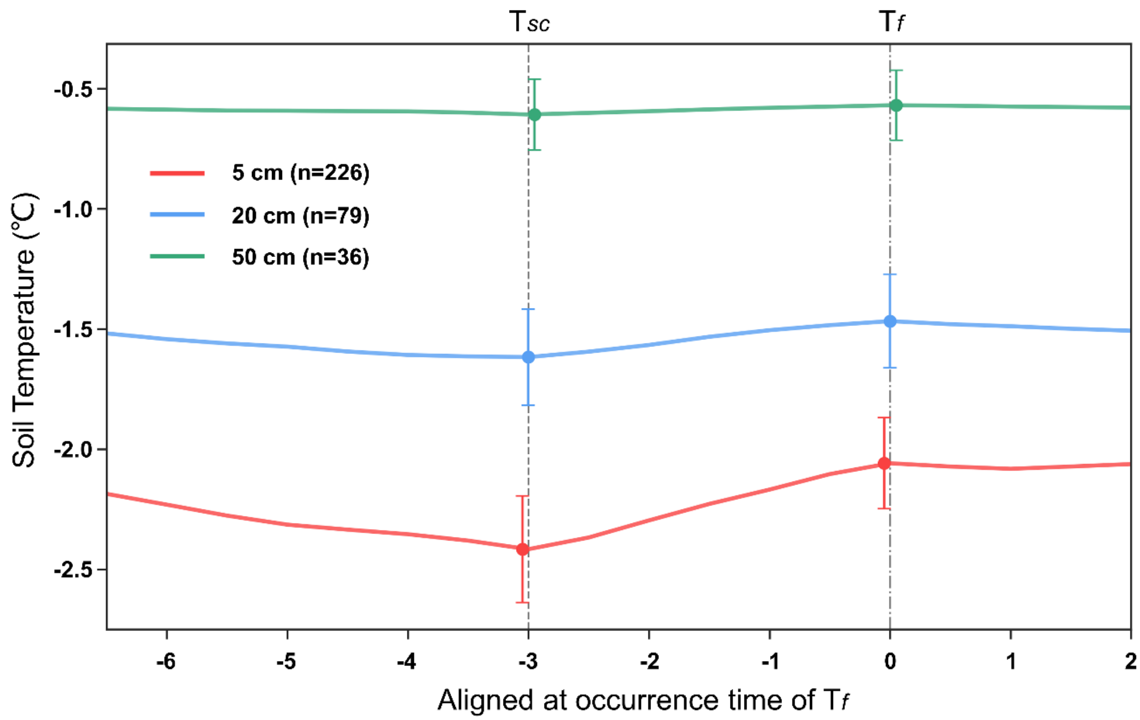

Supplementary Fig. 13 Soil temperature evolution curves of nocturnal freezing processes at different depths. Composite soil temperature curves aligned at T_f for nocturnal freezing events with a fixed 3-hour time lag between T_{sc} and T_f, shown for different soil depths. Numbers denote the total number of independently identified latent heat release events.

Supplementary Tables

Supplementary Table 1. Monthly number, occurrence temperatures and their standard deviation of different types of SUS events.

Month	Class	Number of events		Mean surface temperature	Std	Mean soil temperature		Std	
		6:00	18:00			6:00	18:00	6:00	18:00
1	CT	1,696,027	1,677,879	269.37	6.96	269.18	269.56	4.31	3.89
1	DFT	1,334,827	1,427,231	268.1	6.42	267.83	268.34	4.83	4.31
1	FP	527,372	579,988	268.7	4.3	268.64	268.76	4.31	4.28
1	TP	572,374	515,070	268.69	4.33	268.47	268.94	4.55	4.04
2	CT	1,679,161	1,617,744	269.59	6.95	269.43	269.76	3.94	3.6
2	DFT	1,059,930	1,299,110	268.46	5.73	268.04	268.79	4.4	3.9
2	FP	441,852	509,702	269.04	3.85	268.83	269.23	3.96	3.66
2	TP	506,602	506,868	268.94	3.98	268.68	269.19	4.14	3.68
3	CT	5,816,277	5,068,311	269.74	11.83	269.48	270.03	10.26	9.71
3	DFT	1,550,532	3,159,496	268.7	9.26	268	269.05	4.59	7.31
3	FP	875,604	1,263,723	269.03	4.58	268.69	269.27	3.98	3.59
3	TP	996,655	1,444,573	269.06	5.29	268.54	269.42	4	3.51
4	CT	11,976,685	9,651,967	271.28	43.64	271.05	271.55	12.64	11.93
4	DFT	399,869	2,067,455	270.65	4.16	269.81	270.81	3.18	2.59
4	FP	437,133	1,123,753	270.95	2.56	270.49	271.13	2.91	2.38
4	TP	507,068	1,357,461	270.89	2.55	270.24	271.13	2.89	2.36
5	CT	4,315,369	2,507,681	272.5	10.68	272.4	272.66	6.97	0.85
5	DFT	27,400	492,764	272.2	1.22	271.25	272.26	2.12	1.13
5	FP	51,243	229,913	272.34	1.25	271.92	272.44	1.7	1.08
5	TP	54,647	298,412	272.45	1.13	271.9	272.55	1.67	0.97
6	CT	83,281	17,319	272.94	0.46	272.92	273.06	0.47	0.16
6	DFT	394	4,330	272.9	0.43	272.31	272.96	1.09	0.23
6	FP	730	2,260	272.85	0.46	272.66	272.92	0.74	0.29
6	TP	721	2,074	272.85	0.63	272.42	273	1.08	0.2

7	CT	125	1	273.07	0.11	273.07	273.05	0.11	
7	DFT	0	2	273.04	0.04		273.04		0.04
7	FP	0	4	273.06	0.02		273.06		0.02
7	TP	1	3	273.08	0.03	273.12	273.06		0.02
8	CT	154	40	272.79	0.52	272.72	273.04	0.57	0.1
8	DFT	4	8	272.99	0.21	272.88	273.04	0.29	0.15
8	FP	5	3	272.46	0.67	272.37	272.61	0.79	0.55
8	TP	14	4	272.82	0.42	272.73	273.12	0.44	0.03
9	CT	159,395	69,420	271.98	1.52	271.73	272.53	1.68	0.75
9	DFT	7,413	26,496	272.15	1.23	271.36	272.37	1.84	0.88
9	FP	9,442	18,795	272.14	1.22	271.56	272.42	1.6	0.84
9	TP	9,680	13,467	272.15	1.32	271.62	272.53	1.69	0.76
10	CT	4,587,561	2,922,143	271.33	11.67	270.98	271.88	9.34	3.78
10	DFT	778,484	1,375,119	270.79	2.71	270.03	271.22	2.9	2.07
10	FP	647,161	850,265	271.07	2.24	270.45	271.53	2.56	1.81
10	TP	593,673	684,195	271.19	2.29	270.69	271.62	2.5	1.82
11	CT	3,824,074	3,314,180	269.82	10.87	269.45	270.24	8.11	6.71
11	DFT	2,064,296	2,405,351	268.69	9.24	268.29	269.04	5.28	5.48
11	FP	1,039,266	1,081,534	269.39	4.48	269.06	269.7	4.3	3.82
11	TP	983,366	961,269	269.44	4.15	269.19	269.69	4.34	3.88
12	CT	2,340,428	2,292,776	269.18	9.08	268.83	269.55	5.66	5.02
12	DFT	1,964,451	2,080,983	267.93	8.62	267.68	268.17	5.71	5.49
12	FP	783,559	801,499	268.57	5.05	268.37	268.76	5.13	4.85
12	TP	796,886	751,438	268.67	4.96	268.47	268.87	5.1	4.7

Supplementary Table 2. XGBoost classification and regression model performance.

Classification	Accuracy	Precision	Recall	AUC
6:00	98.35571	0.985457	0.9818	0.998786
18:00	98.27714	0.984571	0.981143	0.998786
Regression	MSE	MAE	R^2	
6:00	1.061157	0.612929	0.926543	
18:00	0.845843	0.557129	0.930314	

Supplementary Table 3. Soil freezing point (T_f), standard deviation (std) and temperature difference between freezing point and supercooling temperature (T_{sc}) caused by latent heat release. Statistical characteristics of all FP events identified at 6:00 and 18:00 from SMAP satellite records (2015-2022) (see Methods).

18:00	Median	Mean	06:00	Median	Mean
T_f	271.50	270.28	T_f	271.03	269.62
T_f std	3.36		T_f std	4.04	
T_f-T_{sc}	0.13	0.12	T_f-T_{sc}	0.87	0.80

Supplementary Table 4. Soil freezing point (T_f), standard deviation (std), and kernel density estimation peak temperature (KDE peak). Statistical characteristics of freezing events identified from thermodynamically consistent temperature trajectories at 18:00 derived from 19 collocated pairs of SMAP satellite pixel time series and in-situ observations from eddy covariance flux towers (see Methods for details).

18:00	In-situ		Satellite-derived	
	Median	Mean	Median	Mean
T_f	272.01	270.24	271.65	270.80
T_f std	3.85		2.35	
KDE peak	272.37		272.57	

Supplementary Table 5. Source of the Dataset for This Study.

Variable	Source	Type	Time step	Remark	Link
Freeze-thaw State	SPL3FTP_E	Satellite	12-hour	Local Solar Time	https://nsidc.org/data/spl3ftp_e/versions/4
Surface temperature					
Soil temperature	SPL4SMAU	Satellite	3-hour	UTC Time	https://nsidc.org/data/spl4smau/versions/7
Soil moisture					
Soil temperature	ERA5-Land	Model	1-hour	UTC Time	https://cds.climate.copernicus.eu
TS_F_MDS_x					
SWC_F_MDS_x	FLUXNET	In-situ	1-hour	Local Solar Time	https://ameriflux.lbl.gov https://doi.org/10.18160/2G60-ZHAK
G_F_MDS					
Sand, Silt, Clay					
Permanent Wilting Point					
Soil Organic Carbon	Soilgrids	Model	-	-	https://www.isric.org/explore/soilgrids/faq-soilgrids-2017
Cation Exchange Capacity					

SI References

1. Feng, S. et al. Miscellaneous methods for determination of unfrozen water content in frozen soils. J. Hydrol. 631, 130802 (2024).
2. Zhou, J., Wei, C., Lai, Y., Wei, H. & Tian, H. Application of the generalized Clapeyron equation to freezing point depression and unfrozen water content. Water Resour. Res. 54, 9412–9431 (2018).
3. Wang, C. et al. Study on the supercooling characteristics of freezing soil based on nucleation theory. Water Resour. Res. 59, e2023WR034800 (2023).
4. Muñoz Sabater, J. ERA5-Land hourly data from 1950 to present. Copernicus Climate Change Service (C3S) Climate Data Store (CDS) (2019).